Research on Engineering Structures & Materials
www.jresm.org
MIM Research Group

Research Article

Experimental evaluation of the mechanical performance and compressive stress–strain response of normal-strength concrete incorporating densified silica fume and local materials

Salam Naji Hussein [*,1,a], Alyaa Abdulrazzaq Azeez [2,b], Ammar A. Alasadi [3,c]

[1]*Department of Civil Engineering, University of Kufa, Iraq*
[2]*Ministry of Education, Najaf, Iraq*
[3]*Civil Engineering Department, College of Engineering, University of Thi-Qar, Iraq*

Article Info

Article History:

Received 09 July 2026
Accepted 14 Aug 2026

Keywords:

Normal-strength concrete;
Densified silica fume;
Local materials;
Workability;
Compressive stress–strain response;
Apparent secant modulus;
Interfacial transition zone

Abstract

In this study, the effect of densified silica fume on the fresh properties, mechanical performance, and ascending compressive stress-strain response of normal-strength concrete using local Iraqi materials was investigated. Densified Sika® Fume S92 D was used as the replacement for Portland cement at 10% and 15% by total binder mass. Three mixtures were studied: control concrete (NC), concrete containing 10% silica fume (SF10), and concrete containing 15% silica fume (SF15). The total binder content and water-to-binder ratio were kept at 350 kg/m^3 and 0.55, respectively, without chemical admixtures. The slump increased from 130 mm for NC to 180 mm for SF10 and 160 mm for SF15. While this is in contrast to the commonly reported decrease in workability of silica fume, it could be due to the combination of saturated surface dry aggregates, high effective water content, very fine Zone 4 sand, and an incomplete deagglomeration of the densified silica fume. No visible bleeding or aggregate segregation was observed during the workability test. The compressive and splitting tensile strengths of SF15 increased by 22.6% and 24.0%, respectively, compared to NC. The peak compressive stress of the instrumented cylinders increased from 24.0 MPa for NC to 28.2 MPa for SF10 and 33.8 MPa for SF15, while the corresponding peak strain was increased from 0.00102 to 0.00116 and 0.00126. The secant modulus at 40% of peak stress also increased from 32.3 GPa for NC to 36.0 GPa for SF10 and 42.8 GPa for SF15. The descending branches of the SF10 and SF15 curves were not captured reliably, and therefore, no reliable conclusions could be drawn regarding ductility or post-peak behavior. In this range, SF15 had the best overall mechanical performance.

1. Introduction

Rapid urban development, population growth, and expanding infrastructure are factors that are driving the global demand for concrete. Thus, there has been extensive research on the improved performance and material efficiency of concrete when additional cementitious ingredients and other minerals are added.

In the 1970s, silica fume became a key mineral to make denser and stronger cementitious compounds in concrete by virtue of its very fine particles, which can fill the voids between cement grains and improve particle packing. In the presence of calcium hydroxide, silica reacts with the cement paste and forms an additional C-S-H gel. These processes densify and refine the interfacial transition zone (ITZ) between the cement paste and aggregate [1-3]. This microstructural

*Corresponding author: salamn.alamri@uokufa.edu.iq
[a]orcid.org/0009-0000-6211-3404; [b]orcid.org/0000-0002-0236-7538; [c]orcid.org/0009-0004-3388-9827
DOI: http://dx.doi.org/10.17515/resm2026-1847me0709rs

refinement can lead to stronger compressive and tensile strength and stiffness before peak. As the compressive stress-strain response is a fundamental input to structural analysis and constitutive modeling, the effect of silica fume on peak stress, peak strain, and pre-peak deformation should be examined in-depth [4,5].

Silica fume normally enhances the cohesiveness of the mixture and water consumption due to the relatively small size and high specific surface area of the particles. When the water content and chemical-admixture dosage do not differ, silica fume is generally used to reduce slump and slump retention. The effect is dependent on the silica-fume form, degree of deagglomeration, cement/aggregate properties, water-to-binder ratio, and the order of mixing. Therefore, high-range water-reducing admixtures are usually used to improve dispersion and workability of the material [1,6-8]. In hardened concrete, silica fume can improve tensile strength and resistance to transport-related deterioration by refining pores and strengthening ITZ. The C-S-H gel is produced by the pozzolanic reaction of reactive silica with calcium hydroxide, and it increases matrix density and mechanical resistance in a matrix [3,8-10].

However, the performance of silica-fume concrete depends on the cement, aggregates, silica-fume product, mixture proportions, dispersion process, and curing process. As a result, results obtained using one constituent-material system cannot be generalized to another. In the present work, two commonly used replacement levels of densified silica fume were investigated in normal-strength concrete made from locally available Iraqi materials with emphasis on fresh state behavior and strength development, as well as on the ascending compressive stress-strain response at a constant nominal water-to-binder ratio.

1.1 Research Gap and Contribution

Although silica-fume concrete has been investigated thoroughly, the fresh and mechanical response of normal-strength concrete is strongly dependent on cement, aggregates, water content, silica-fume form, and mixing process. The interaction of densified silica fume with locally available Iraqi constituent materials, particularly the Zone 4 fine aggregate used in the present work, has not been adequately demonstrated by a combined evaluation of workability, strength development, splitting tensile strength, and compressive stress–strain behavior. This study provides a controlled experimental dataset for normal-strength concrete produced with local materials and two practical silica-fume replacement levels.

The study examined the compatibility of densified silica fume with local cement and aggregates at a constant total cementitious material content (cement + silica fume) and water-to-binder ratio. The fresh-state slump, compressive-strength development, splitting tensile strength, ascending compressive stress-strain response, peak stress, peak strain, and apparent pre-peak stiffness were assessed. The post-peak branches of silica-fume mixtures were not adequately captured. The stress-strain results were only given for the increasing response and peak parameters.

1.2 Objective

- To evaluate the impact of 10% and 15% densified silica fume replacement on the measured slump of normal-strength concrete made of local materials;
- To determine the effects of silica fume on compressive-strength development at 7 and 28 days
- To evaluate the 28-day splitting tensile strength and its relationship with compressive strength.
- To investigate the ascending compressive stress-strain response, peak stress, peak strain, and apparent secant modulus of the mixtures; and assess the trade-off between fresh-state flowability and hardened mechanical properties within the considered replacement range.

2. Materials and Experimental Program

2.1 Constituent Materials

2.1.1 Cementitious Materials

Ordinary Portland Cement (OPC) manufactured by Saman Cement and supplied locally in Najaf, Iraq, was used as the main binder during the whole study. The cement conforms with IQS No. 5/2019 of the Iraqi standard. The manufacturer reported chemical composition of 21.0% SiO_2, 5.0% Al_2O_3, 3.8% Fe_2O_3, 63.4% CaO, 2.3% MgO, 2.5% SO_3, 0.22% Na_2O, 0.50% K_2O, and 1.6% loss on ignition (LOI). The silica fume (Sika® Fume S92 D) was used to replace cement at 10% and 15% in total binder mass. The product has a particle size below 1 μm, a specific gravity of 2.22, a bulk density of 130–430 kg/m^3, and a specific surface area of 13,000–30,000 m^2/kg. The physical and chemical properties of the cement and silica fume are summarized in Table 1.

Table 1. Physical and chemical properties of Ordinary Portland Cement and densified silica fume

Property	OPC	Silica fume (SF) (Sika® Fume S92 D)
Standard	IQS No. 5/2019	ASTM C1240
Cement type	Ordinary Portland Cement	Densified silica fume
Specific gravity	3.15*	2.22
Blaine fineness	317 m^2/kg	—
Particle size	—	<1 μm
Bulk density (kg/m^3)	—	130–430
Specific surface area (m^2/kg)	—	13,000–30,000
SiO_2 (%)	21.0*	90–95
Al_2O_3 (%)	5.0*	0.5–0.8
Fe_2O_3 (%)	3.8*	0.07–1.9
CaO (%)	63.4*	0.50
MgO (%)	2.3*	0.04–0.90
Na_2O (%)	0.22*	0.30–0.42
K_2O (%)	0.50*	0.50–1.30
SO_3 (%)	2.5*	—
LOI (%)	1.6*	≤6.0 **
Moisture content (%)	—	≤3.0 **

**Cement values are manufacturer-reported results for Saman Ordinary Portland Cement.*
*** Product-specific LOI and moisture values for Sika® Fume S92 D were not available; therefore, the ASTM C1240 acceptance limits are reported and are not presented as measured values.*

2.1.2 Aggregate

The particle size distributions of the fine and coarse aggregates were determined by sieve analysis. As shown in Figures 1 and 2, the fine aggregate was within the grading limits of Zone 4, and the natural coarse aggregate was within the grading range of 5-14 mm according to Iraqi Standard Specification IQS No. 45/1984. The nominal maximum size of the coarse aggregate was 14 mm. The cylinder diameter-maximum aggregate size ratio was approximately 7.1 and 10.7 for the 100 and 150 mm diameter specimens, respectively. Both cylinder sizes provided dimensions well above the minimum commonly required relative to the nominal maximum aggregate size. The physical properties of the aggregates are summarized in Table 2.

Table 2. Physical properties of the fine and coarse aggregates.

Property	Fine aggregate	Coarse aggregate
Specific gravity	2.68	2.59
Water absorption (%)	0.64	1.03
Loose unit weight (kg/m^3)	1528	1396
Compacted unit weight (kg/m^3)	1689	1568

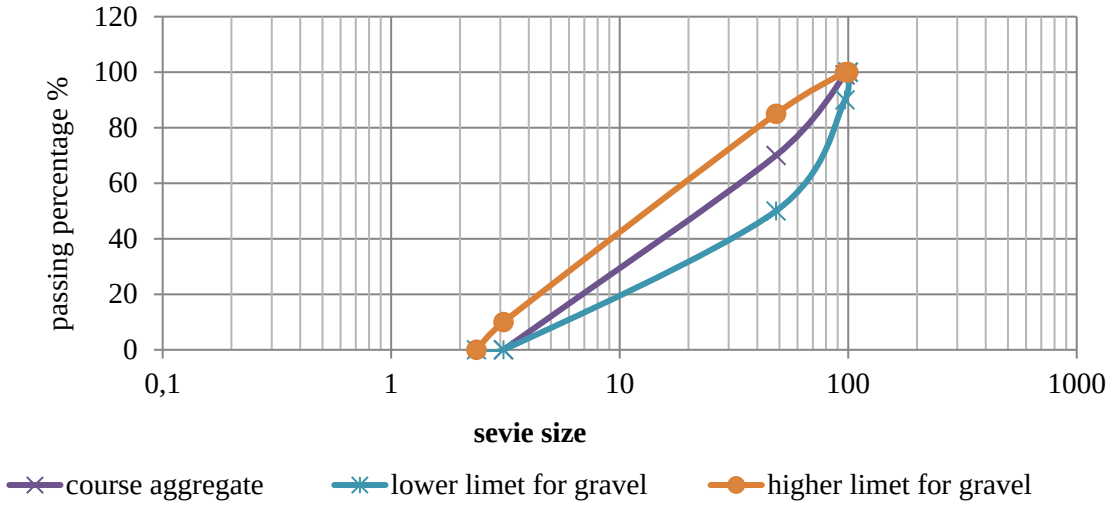

Fig. 1. Particle-size distribution of the coarse aggregate compared with the grading limits for Zone 5–14 according to IQS No. 45/1984

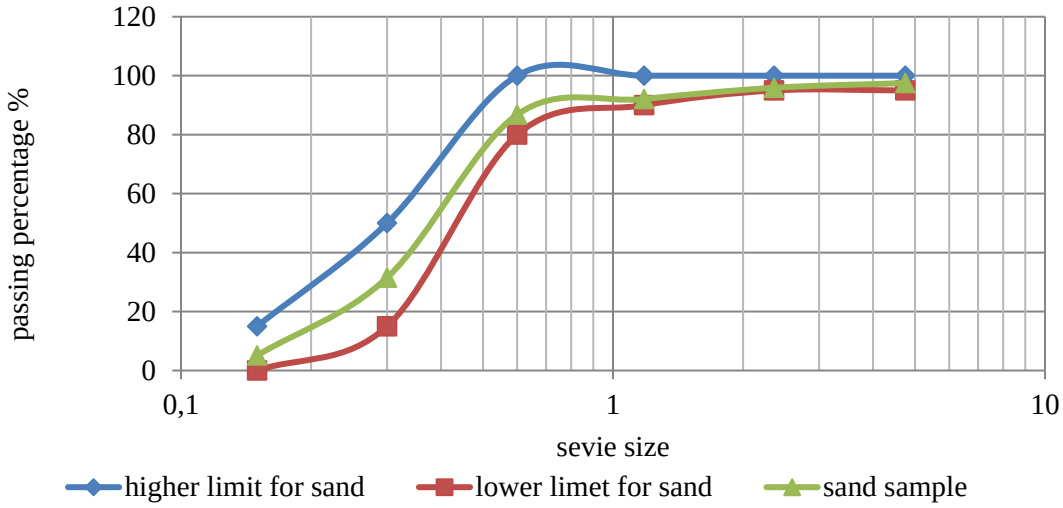

Fig. 2. Particle-size distribution of the fine aggregate compared with the grading limits for Zone 4 according to IQS No. 45/1984

2.2 Mixture Proportions

Three mixtures were considered:

- Control concrete with zero content of silica fume (NC);
- Concrete with 10% silica fume as a replacement of cement. (SF10).
- Concrete with 15% silica fume as a replacement of cementt (SF15).

The total binder content was kept at 350 kg/m3 for all mixtures. Therefore, silica fume was considered as a partial cement replacement and not as an additional powder. The water content was kept at 192.5 kg/m3 maintaining a constant water-to-binder ratio of 0.55. Before mixing, the fine and coarse aggregates were brought to the saturated surface-dry condition. Thus, no mixing water was needed for aggregate absorption, and the effective water-to-binder ratio was 0.55.

The water-to-binder ratio was maintained to study the effect of silica-fume replacement and particle packing without changing the nominal water content. The quantities in Table 3 are the actual batched proportions. Since cement was replaced with lower-density silica fume, the absolute

binder volume slightly increased. By using specific gravities of the model, the nominal absolute yields were around 1.036 m^3 for NC, 1.041 m^3 for SF10, and 1.043 m^3 for SF15 for the nominal 1.0 m^3 batch. The mass-based w/b ratio was therefore 0.55, but the uncorrected yield slightly decreased the total content of the constituent and weight per actual cubic meter. The effect was small and systematic, but it is acknowledged as a limitation when comparing mechanical properties.

Table 3. Concrete mixture proportions used in this study

Mixture	Cement (kg/m3)	Silica fume (kg/m3)	Fine aggregate *(kg/m^3)	Coarse aggregate (kg/m^3)*	Water (kg/m^3)	w/b
NC	350.0	0.0	670	1250	192.5	0.55
SF10	315.0	35.0	670	1250	192.5	0.55
SF15	297.5	52.5	670	1250	192.5	0.55

** The fine and coarse aggregates were used in the saturated surface-dry (SSD) condition. Hence, the reported water content is the effective mixing water, and the water-to-binder ratio was maintained at 0.55.*

The replacement percentage was calculated as the mass of silica fume divided by the total binder mass, as shown in Eq. (1).

$$SF\ replacement\ (\%) = [SF / (C + SF)] \times 100 \quad (1)$$

Where SF is the silica fume content in kg/m^3, C is the cement content in kg/m^3.

2.3 Mixing Procedure

The mixing procedure is shown in Figure 3. For each mixture the quantities were weighed before mixing to produce a nominal batch volume of 0.25 m^3. Before batch mixing, the mixer drum was washed and wiped with a clean, dry towel to remove free water and maintain a uniformly damp internal surface. Cement and silica fume were first dry-blended to ensure a uniform distribution before being added to the total mixture.

2.4 Specimen Preparation and Curing

For each mixture, twelve cylinders were prepared. The steel molds were cleaned and lightly oiled before casting. After casting and compaction, the specimens were covered to minimize moisture loss and stored in the molds for 24 h. They were then demoulded and fully immersed in tap water maintained at 23 ± 2°C until the designated testing age. Because the specimens were submerged, the curing condition was treated as a saturated environment; ambient relative humidity was therefore not a controlling curing parameter. The specimens were removed immediately before testing, and excess surface water was wiped off. The preparation and curing sequence is shown in Figure 4.

2.5 Test Methods

- Workability was evaluated by slump test according to ASTM C143/C143M [11].
- The compressive strength testing was performed with cylinders measuring 150 × 300 mm (ASTM C39/C39M [12]), and the splitting-tensile strength testing with cylinders measuring 100 × 200 mm (ASTM C496/C496M [14] and compressive stress-strain response following the axial deformation measurement of ASTM C469/C469M [13]).

Mechanical tests were done with a compression testing machine had a maximum ultimate load of 2000 kN. The load was applied in continuous form at a stress rate of 0.25 ± 0.05 MPa/s, as per ASTM C39/C39 M. The splitting tensile load was applied continuously at the ASTM C496/C496M splitting-stress of 0.7-1.4 MPa/min rate of loading. The stress-strain cylinders were loaded under force control by the same continuous ASTM C39/C39M loading rate while axial deformation was measured.

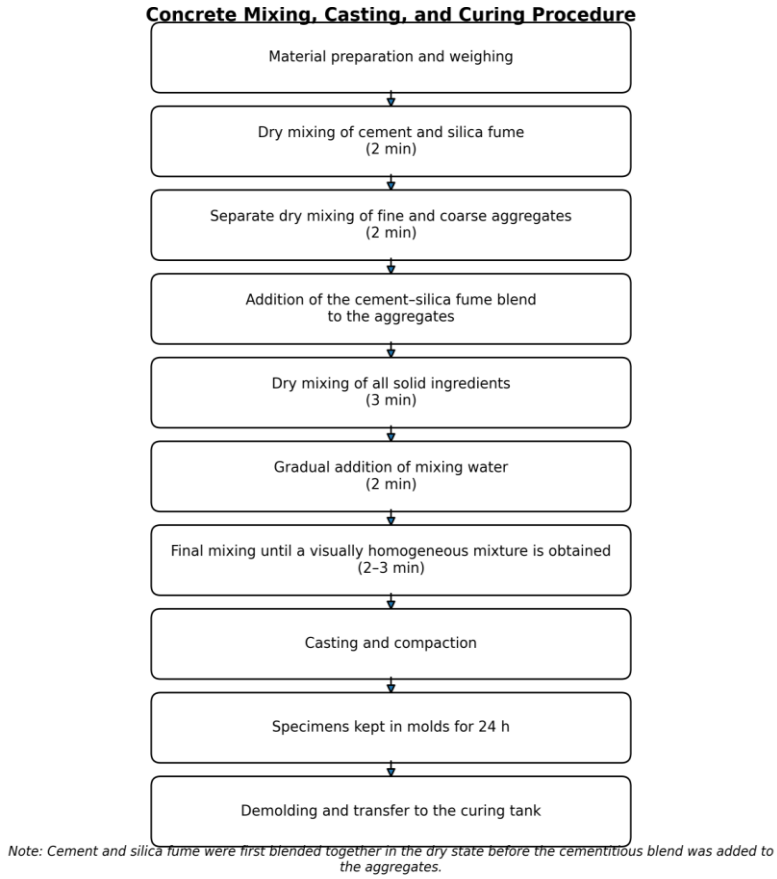

Fig. 3. Mixing procedure of concrete

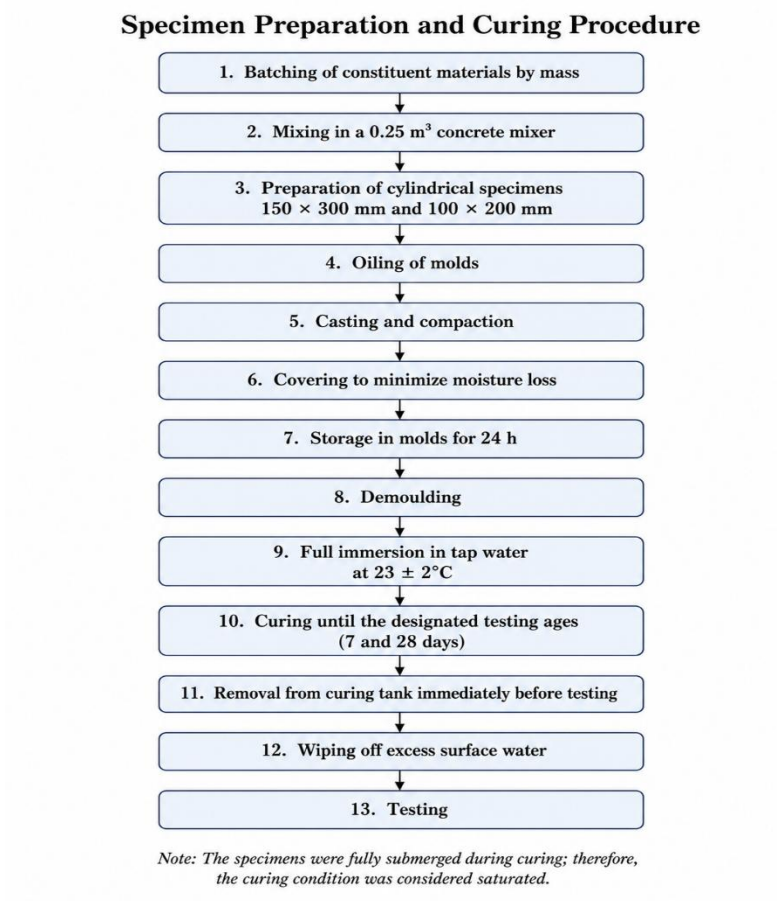

Fig. 4. Specimen preparation and curing procedure

The numbers of testing specimens was three for each mixture and age. The specimens were tested for compressive and splitting tensile strengths being averages for the three specimens. Three separate 100 × 200 mm instrumented cylinders were used for the compressive stress-strain measurements. Axial deformation during the compressive stress-strain test was measured using an external yoke system with a laser displacement sensor. The sensor measured relative axial displacement between the two yokes during loading, and the axial strain was calculated by dividing the measured displacement by the gauge length. The setup is consistent with the general ASTM C469/C469M approach to measuring axial deformation; however, the resulting modulus values are observed in the form of apparent secant moduli rather than standard ASTM chord moduli. The percentage improvement to the control mixture was evaluated using Eq. (2).

$$Improvement\ (\%) = [(X\_SF - X\_NC) / X\_NC] \times 100 \quad (2)$$

Where; X_SF is the measured property of a silica-fume mixture, X_NC is the corresponding value of the control mixture at the same age.

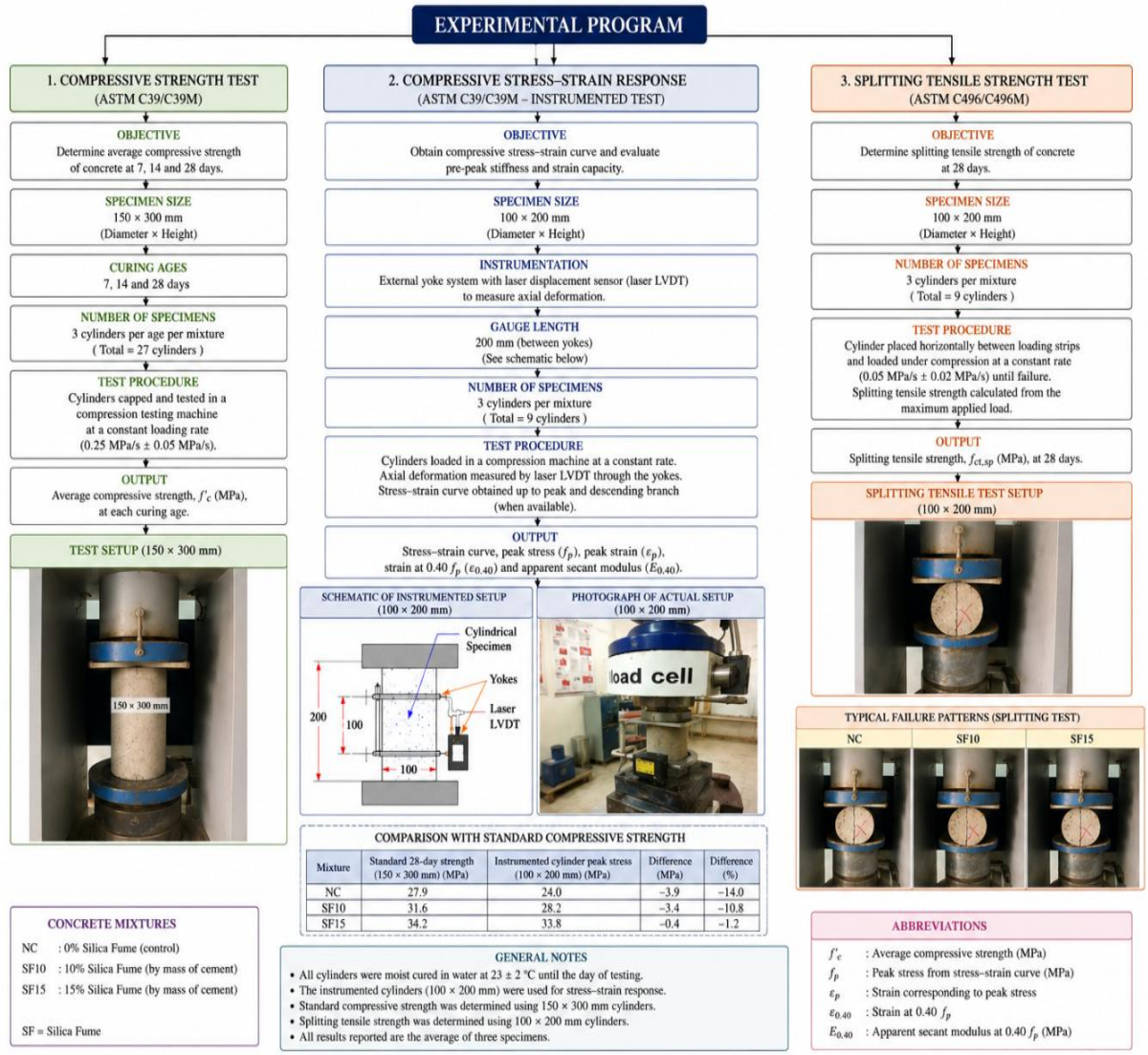

Fig. 5. The main stages of methodology program.

For splitting tensile strength, the standard expression is given by Eq. (3).

$$fct,sp = 2P / (\pi DL) \quad (3)$$

Where; fct,sp is the splitting tensile strength in MPa, P is the maximum applied load in Newton, L is the cylinder length in mm, D is the cylinder diameter in mm.

To provide a concise visual summary of the experimental methodology adopted in this study, a process flow chart of the experimental program is presented in Figure 5.

3. Results and Discussion

3.1 Workability

The slump results are shown in Table 4 and Figure 6. NC had a slump of 130 mm, while SF10 and SF15 were at 180 and 160 mm, respectively, which is 38.5% and 23.1%. Thus, SF10 had a higher slump than SF15. The higher slump of the silica-fume mixtures was not expected, as the fully dispersed silica fume is responsible for the high water demand and cohesiveness of the mixture because of the very high specific surface area of the silica fume, but it has to be explained by more than one material and processing effect, such as:

- The aggregates were in the saturated surface-dry (SSD) condition, and so did not absorb a significant amount of 192.5 kg/m^3 mixing water in the aggregate skeleton.
- The high number of fine particles in Zone 4 sand may have increased the volume and continuity of the mortar phase and influenced the mobility and water distribution of the fresh mixture.
- Most importantly, densified silica fume needs to be efficiently deagglomerated. If there were no superplasticizer, some of the densified particles may have remained as larger agglomerates rather than as individual ultrafine particles. This would have diminished the effective surface area exposed to water during the short slump-test period and may temporarily lower the water demand.
- The Sika technical advice also provides that superplasticizers promote deflocculation and uniform distribution of Sika Fume S92 D [15].

Such mechanisms are physically plausible but not directly proven, as no particle dispersion, rheology, or pore-water distribution was observed. Thus, the increase should not be characterized as a general ball-bearing effect or a general effect of the silica-fume addition. Rather, it is a mixture-specific response to the combination of SSD conditions, high effective water content, fine aggregate grading, or incomplete deagglomeration of the densified product. Despite the 180 mm slump of SF10, there was no bleed-water accumulation, coarse aggregate settlement, or mortar separation during the slump test or handling. This was qualitative because no bleeding and segregation resistance tests were performed. By increasing the replacement level from 10% to 15%, the slump was reduced from 180 to 160 mm. This is consistent with the greater quantity and total surface area of ultrafine silica-fume particles in SF15, which would be expected to increase water demand and reduce the amount of free water available for flow.

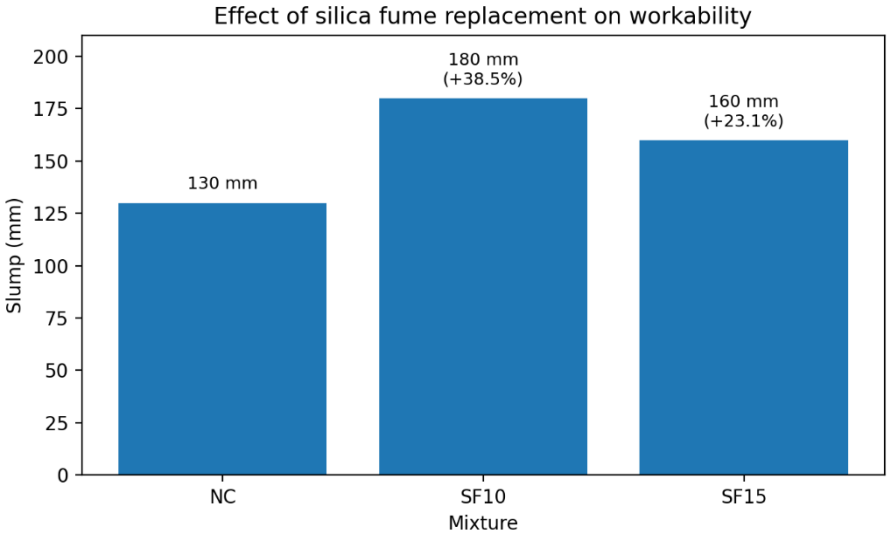

Fig. 6. Effect of silica fume replacement on concrete slump

Table 4. Slump results and percentage change relative to the control mixture.

Mixture	Slump (mm)	Change relative to NC (%)
NC	130	0
SF10	180	38.5
SF15	160	23.1

3.2 Compressive Strength Development

The strong compressive strength of silica fume was due to physical and chemical effects. At early ages, ultrafine particles can fill spaces between cement grains and provide nucleation sites for hydration products. This leads to denser particle packing and precipitation of hydration products. So the early-age strength is much stronger, even for the partial replacement of cement. At later ages, the pozzolanic reaction becomes more important. Silica fume reacts with calcium hydroxide released during cement hydration and forms a calcium-silicate-hydrate (C-S-H) gel. As a result, the secondary C-S-H gel reduces capillary porosity, improves the pore structure, and improves the ITZ between cement paste and aggregate. Combined filler, nucleation, and pozzolanic effects account for the higher 28-day compressive strength of silica-fume mixtures.

SF15 had the highest compressive strength at both testing ages. The 28-day strength was 6.3 MPa higher than NC and 2.6 MPa higher than SF10. Therefore, of the replacement levels studied, 15% silica fume had the highest compressive strength. This should be seen in the context of the present mixture and should not be considered as the universal optimum silica-fume content. The 28-day to 7-day strength ratios were 1.69 for NC, 1.74 for SF10, and 1.70 for SF15. The very close ratios indicate that all mixtures had relatively similar strength development patterns in the period in question. However, the strength increase of the silica-fume mixtures at 7 days despite the reduced cement content suggests that the early physical filler and nucleation effect was already considerable. The slightly higher ratio of SF10 might indicate a slightly greater relative contribution from the later-age pozzolanic activity, while the high early strength of SF15 resulted in a 28/7 ratio closer to the control mixture.

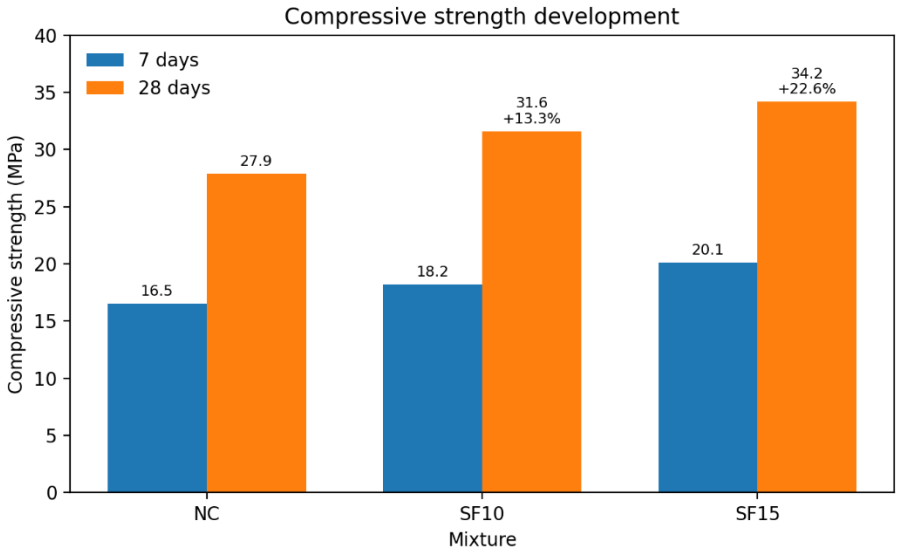

Fig. 7. Compressive strength development of control and silica-fume concrete mixtures

Since the aggregates were used in the saturated surface-dry condition, significant absorption of the designed mixing water was avoided. Therefore, the early-age strength increase should not be directly attributed to a significant reduction in the overall effective water-to-binder ratio. Nevertheless, local particle packing and water distribution in the paste may have influenced hydration and microstructural development, although these effects were not measured directly.

Table 5. Compressive strength results and calculated improvement indices.

Mixture	7-day f'c (MPa)	Change relative to NC (%)	28-day f'c (MPa)	Change relative to NC (%)	28/7 strength ratio
NC	16.5	0.0	27.9	0.0	1.69
SF10	18.2	10.3	31.6	13.3	1.74
SF15	20.1	21.8	34.2	22.6	1.70

3.3 Splitting Tensile Strength Development

The 28-day splitting tensile strength results are shown in Table 6 and Figure 8. NC achieved 2.5 MPa, while SF10 and SF15 achieved 2.9 and 3.1 MPa, respectively. This led to increases of 16.0% and 24.0%, respectively, compared to NC. The splitting tensile strength has been improved through the physical and chemical effects of silica fume on the hardened matrix and the ITZ.

The dense particles can fill micro voids and enhance the packing of aggregate surfaces, and the pozzolanic reaction gives rise to additional C-S-H gel and reduces weak porous areas in the ITZ. The experimental splitting-to-compressive-strength ratios were 8.96% for NC, 9.18% for SF10, and 9.06% for SF15. Their narrow range indicates that tensile strength increased in general in conjunction with compressive strength, and it is likely that ITZ refinement was part of the reason for the improvement. SF10 had the highest tensile-to-compressive-strength ratio, while SF15 had the highest absolute splitting tensile strength.

Table 6. Experimental splitting tensile strength.

Mixture	Experimental fct,sp (MPa)	Change relative to NC (%)	fct,sp/f'c (%)
NC	2.5	0.0	8.96
SF10	2.9	16.0	9.18
SF15	3.1	24.0	9.06

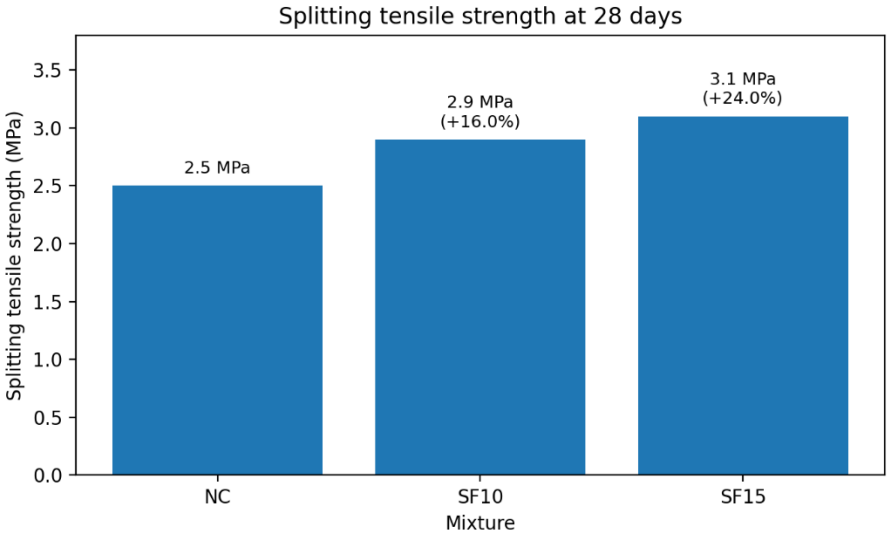

Fig. 8. Splitting tensile strength at 28 days

As shown in Figure 9, the fresh and hardened-state results exhibited different trends with increasing silica-fume replacement. The response was therefore not monotonic but independent of the replacement level. SF10 had the highest slump measured, whereas SF15 had the highest compressive and splitting tensile strengths.

The low slump of SF15 compared to SF10 is consistent with the higher quantity and total surface area of ultrafine silica-fume particles, which can increase water demand. In contrast, the higher compressive and tensile strength of SF15 indicates that greater contributions from particle

packing, matrix refinement, pozzolanic reaction, and the interfacial transition zone are observed. These results demonstrate the trade-off between fresh state flowability and hardened mechanical performance for the replacement range. SF10 exhibited the highest slump, and SF15 showed the strongest overall mechanical response. However, because the slump increases are unusual and no quantitative rheological or stability tests were performed, SF10 is not the best in terms of workability. It is more accurate to say that SF10 had the highest slump under the present experimental conditions. The results should not be taken as a universal optimum silica-fume content. The ideal replacement level is based on the combination of fresh-state handling, mechanical strength, durability, cost, and field placement.

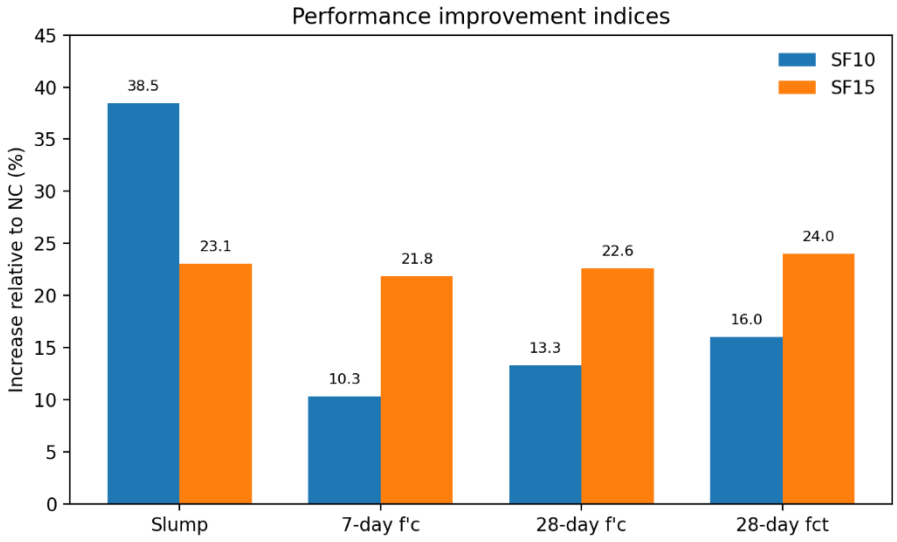

Fig. 9. Improvement indices relative to the control mixture

3.4 Stress–Strain Response

The compressive stress-strain curves of NC, SF10, and SF15 are shown in Figure 10. The curve for each mixture is the average response from separately cast 100 × 200 mm instrumented cylinders. The axial deformation was measured with an external yoke system with a laser displacement sensor, and the recorded displacement was divided by the gauge length to calculate the axial strain. The three mixtures showed the same behavior in the first ascending region, and the curves became more separated at higher stress levels. The rising response of silica-fume mixtures is stronger due to better particle packing, micro void filling, additional C-S-H gel growth and ITZ refinement.. In fact, these mechanisms resulted in a denser, hardened matrix that can withstand a higher compressive stress before the peak.

The post-peak branch was only recorded for the NC mixture. The descending branches of SF10 and SF15 could not be captured reliably with the available testing setup. Thus, the analysis focused on the ascending response, peak stress, peak strain, and the apparent stiffness before peak. This is not an indication of ductility, toughness, energy absorption, or post-peak softening of silica-fume mixtures. The peak stresses produced by the instrumented cylinders were lower than the average 28-day compressive strengths obtained from the standard compression tests. The comparison can be interpreted with caution because the standard compressive-strength specimens were 150 × 300 mm cylinders, and the stress-strain specimens were 100 × 200 mm cylinders. In addition to the specimen sizes and strength, the dataset can be affected by the variability of the specimens, the attachment of instruments to the cylinders, the fit of the instruments, the load conditions, and the data. Because these factors were not studied separately. Since the descending branches of the SF10 and SF15 stress-strain curves were not reliably recorded, only the ascending response was considered. The apparent secant modulus was calculated at 40% of the peak stress using Eq. (4):

$$E0.40 = 0.40fp / \varepsilon 0.40 \quad (4)$$

Where; fp is the peak stress obtained from the instrumented cylinder; and ε0.40 is the axial strain corresponding to 40% of the peak stress.

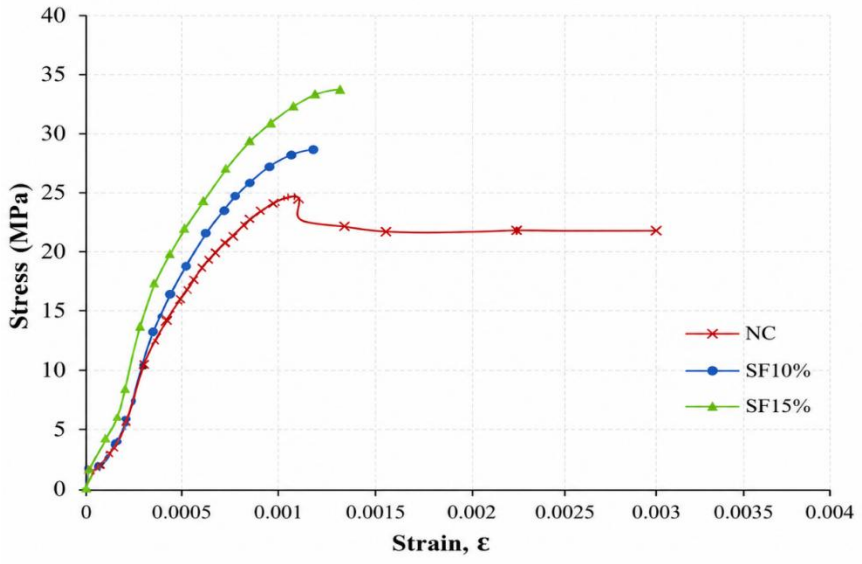

Fig. 10. Compressive stress–strain responses of NC, SF10, and SF15 obtained from instrumented cylinder tests

The increase is attributed to the combined filler effect, better particle packing, additional C-S-H gel formation, and ITZ refinement, which together resulted in a denser and stiffer hardened matrix. However, these values are apparent secant moduli calculated from the recorded stress-strain curves and should not be regarded as ASTM C469/C469M chord-modulus values.

Table 7. Peak parameters and apparent secant modulus at 40% of peak stress

Mixture	Mean values peak stress (MPa)	Mean values peak strain	40% peak stress (MPa)	Strain at 40% peak stress	E0.40 (GPa)	Change relative to NC (%)
NC	24.0	0.00102	9.60	0.000297	32.3	—
SF10	28.2	0.00116	11.28	0.000313	36.0	11.5
SF15	33.8	0.00126	13.52	0.000316	42.8	32.5

3.5 Failure Patterns

The failure patterns for the splitting tensile tests are shown in Figure 11. In all mixtures, the main crack formed along the loaded vertical diameter, as expected from the splitting tensile failure. NC, SF10, and SF15 showed the same principal crack orientation, which indicates that the load is transferred along the expected diametric plane.

The three mixtures have similar splitting structures with a large vertical crack between loading lines. Cracking in the silica-fume mixtures appeared to be relatively localized along the splitting plane. As crack widths and propagation rates were not measured, this comparison is qualitative. The increased splitting strength of the SF10 and SF15 is consistent with a denser cementitious matrix and a better ITZ, but the photographs alone cannot tell whether cracks propagated mainly through the paste and along the aggregate-paste interface or if aggregate particles are involved.

The compressive cylinders cracked with their axial and inclined cracking, followed by local crushing, as shown in Figure 12. Failure was neither sudden nor explosive and was not accompanied by substantial ejection of fragments. The sequence is rather consistent with a columnar/shear failure rather than a perfect cone. No clear transition from gradual to brittle failure was seen with increasing silica-fume content. The higher peak stress and the apparent stiffness of

SF10 and SF15 should therefore not be interpreted as the result of a more brittle or explosive failure mode, as their post-peak branches were not captured reliably.

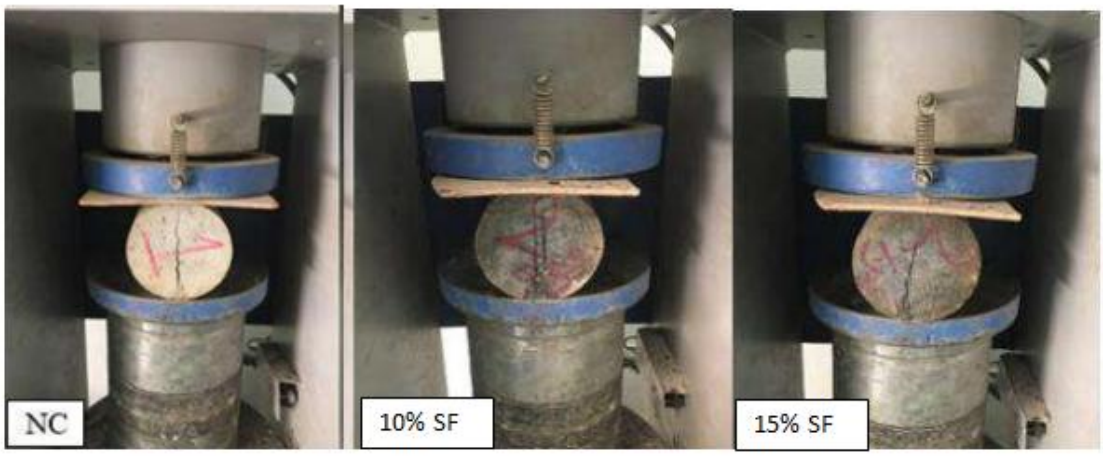

Fig. 11. Splitting tensile failure patterns of the cylinders: (a) NC, (b) SF10, and (c) SF15

Fig. 12. Progressive compressive failure observed during cylinder testing

3.6 Study Limitation

The economic feasibility of silica-fume concrete should be considered. Silica fume is often more expensive than ordinary Portland cement and may increase material cost. Higher strength, on the other hand, may lead to better member dimensions, less binder demand in new mixtures or less maintenance costs.

Due to the lack of a cost analysis, the economic feasibility of silica-fume incorporation could not be established. Although partial cement replacement and better strength may improve material efficiency, the net economic benefit depends on silica-fume cost, transportation, processing, mixture optimization, and potential reductions in structural dimensions or maintenance requirements. This might also lead to lower clinker consumption and hence even less embodied carbon in concrete production, but the environmental benefits will depend on the distance between silica-fume processing and the substitution plan in practice.

The study has several limitations. Only two silica-fume replacement levels, 10% and 15%, were studied. The mechanical properties were examined mainly at 7 and 28 days. Durability, microstructure, drying shrinkage, creep, long-term strength, and field performance were not investigated. In addition, the descending branches of the SF10 and SF15 stress-strain curves were not recorded, which prevented evaluation of post-peak softening, toughness, energy absorption, and ductility.

4. Conclusions

The effect of substituting 10% and 15% Portland cement with densified silica fume on fresh properties, mechanical performance, and the magnitude of compressive stress and strain rise of normal-strength concrete made of local materials was examined. In the replacement range, silica-fume incorporation showed a favorable effect on compressive and splitting tensile strengths at the peak compressive stress, peak strain, and apparent pre-peak stiffness of the sample compared to the control mixture. These benefits were due to the combined filler, particle-packing, nucleation, and pozzolanic properties of the silica fume, which promoted a stronger cementitious matrix that, had fewer internal voids and a better interface between cement paste and aggregate. The main conclusions from this study are as follows:

- Among all mixtures studied, SF15 had the best overall mechanical performance at 7 and 28 days. It showed the highest compressive strength, splitting tensile strength, peak compressive stress, peak strain, and apparent secant modulus. SF10 had good mechanical performance, and also had the highest slump. While SF15 had a lower slump than SF10, its slump was still larger than that of the control mixture. The unusual slump response was considered mixture-specific and might have been due to the combined effects of SSD aggregates, high effective water content, fine-aggregate grading, and incomplete deagglomeration of the densified silica fume. No bleeding or coarse aggregate segregation was observed during mixing, slump testing, or handling. However, this observation was qualitative because no bleeding, segregation-resistance, or rheological tests were performed.
- The compressive stress-strain results showed that silica-fume incorporation enhanced the ascending response and the strain at peak stress as well. The apparent secant modulus also increased as the silica-fume content increased, suggesting a stiffer pre-peak response. However, the descending branches of the SF10 and SF15 curves could not be captured well. This left no reliable conclusions regarding ductility, toughness, post-peak softening, fracture energy, or energy-absorption capacity.
- From a practical point of view, the results suggest that densified silica fume can improve the mechanical efficiency of normal-strength concrete and partially reduce Portland cement content. However, the results should not be taken as a universal optimum replacement level. The performance of silica-fume concrete in terms of material properties, mixture proportions, dispersion efficiency, curing conditions, sample size, and testing procedures should be further investigated. These should include a more diverse range of replacement levels, controlled use of superplasticizers in the production process, rheological and stability measurements, durability tests, microstructural characterization, and displacement-controlled testing to obtain the full post-peak response.

5. Recommendations for Future Research

- Other studies can examine a wider range of silica-fume replacement levels and include mixtures containing superplasticizers to better understand how silica-fume content, dispersion, water demand, and fresh-concrete stability are related. More fresh-state tests (air content, segregation resistance, bleeding, rheological measurements) are recommended to verify the unusual slump behavior in this study.
- Future experiments should also include full displacement-controlled stress-strain tests to capture the descending branch and thus allow for reliable evaluation of ductility, toughness, fracture energy, and constitutive behavior. Microstructural characterization with scanning electron microscopy, X-ray diffraction, or mercury intrusion porosimetry (MIP) would also be useful to validate the proposed filler, pozzolanic, and ITZ-refinement mechanisms.
- Long-term strength, drying shrinkage, creep, permeability, chloride penetration, sulfate resistance, carbonation, and other durability indicators should also be studied. Finally, life cycle and cost analysis is necessary to determine if the mechanical and

environmental benefits of silica-fume replacement justify its additional material and processing costs in field applications.

References

[1] ACI Committee 234. Guide for the Use of Silica Fume in Concrete (ACI PRC-234-06). Farmington Hills, MI: American Concrete Institute; 2006.

[2] ASTM C1240-20. Standard Specification for Silica Fume Used in Cementitious Mixtures. West Conshohocken, PA: ASTM International; 2020.

[3] Wang X, Zhang S, Wang C, Liu L, Wang J. Properties and microstructure of an interfacial transition zone enhanced by silica fume in concrete prepared with coal gangue as an aggregate. ACS Omega. 2023;8:48873–48884. https://doi.org/10.1021/acsomega.3c08560

[4] Shah HA, Nehdi ML, Khan MI, Akmal U, Alabduljabbar H, Mohamed A, Sheraz M. Predicting compressive and splitting tensile strengths of silica fume concrete using M5P model tree algorithm. Materials. 2022;15(15):5436. https://doi.org/10.3390/ma15155436.

[5] Luthfiana H, Wibowo, Safitri E. Study of stress-strain relationship of concrete with silica fume added as partial replacement for cement. Jurnal Teknik Sipil. 2024;24(1):789-799. https://doi.org/10.26418/jts.v24i1.75323.

[6] Mazloom M, Ramezanianpour AA, Brooks JJ. Effect of silica fume on mechanical properties of high-strength concrete. *Cement and Concrete Composites*. 2004;26(4):347–357. https://doi.org/10.1016/S0958-9465(03)00017-9.

[7] Siddique R. Utilization of silica fume in concrete: Review of hardened properties. *Resources, Conservation and Recycling*. 2011;55(11):923–932. https://doi.org/10.1016/j.resconrec.2011.06.012.

[8] Hamada HM, Abed F, Katman HYB, Humada AM, Al Jawahery MS, Majdi A. Effect of silica fume on the properties of sustainable cement concrete. *Journal of Materials Research and Technology*. 2023;24:8887–8908. https://doi.org/10.1016/j.jmrt.2023.05.147.

[9] Zhao S, Sun W, Wu C, et al. Effect of silica fume in concrete on mechanical properties and dynamic behaviors under impact loading. Materials. 2019;12(19):3263.

[10] Gaitero JJ, Campillo I, Guerrero A. Reduction of the calcium leaching rate of cement paste by addition of silica nanoparticles. Cement and Concrete Research. 2008;38(8-9):1112-1118.

[11] ASTM C143/C143M-20. Standard Test Method for Slump of Hydraulic-Cement Concrete. West Conshohocken, PA: ASTM International; 2020.

[12] ASTM C39/C39M-24. Standard Test Method for Compressive Strength of Cylindrical Concrete Specimens. West Conshohocken, PA: ASTM International; 2024.

[13] ASTM C469/C469M-22. Standard Test Method for Static Modulus of Elasticity and Poisson's Ratio of Concrete in Compression. West Conshohocken, PA: ASTM International; 2022.

[14] ASTM C496/C496M-17. Standard Test Method for Splitting Tensile Strength of Cylindrical Concrete Specimens. West Conshohocken, PA: ASTM International; 2017.

[15] Sika. Sika Fume S92 D technical guidance for shotcrete and concrete applications. Sika España; product information accessed 5 August 2026.